Scripta Materialia 259 (2025) 116516

Contents lists available at ScienceDirect

Scripta Materialia

journal homepage: www.journals.elsevier.com/scripta-materialia

A thermodynamic approach to modeling multicomponent FeTi-based alloys for hydrogen storage

Ebert Alvares [a,*], Andrew J.E. Rowberg [a,b], Kai Sellschopp [a], Brandon C. Wood [b], Thomas Klassen [a,c], Paul Jerabek [a,*], Claudio Pistidda [a]

[a] Institute of Hydrogen Technology, Helmholtz-Zentrum Hereon, Max-Planck-Strasse 1, 21502 Geesthacht, Germany
[b] Quantum Simulations Group and Laboratory for Energy Applications for the Future (LEAF), Lawrence Livermore National Laboratory, Livermore, CA 94550, USA
[c] Helmut Schmidt University, Holstenhofweg 85, 22043 Hamburg, Germany

ARTICLE INFO

Keywords:
Substitutional species
FeTi-based alloys
Hydrogen storage
DFT
CALPHAD

ABSTRACT

Modeling the impact of alloying on the hydrogenation properties of intermetallic compounds is a vital yet challenging task for hydrogen storage materials design: not only do these processes occur under thermodynamic para-equilibrium conditions, but for bcc-derived compounds, the task is further complicated through varying composition-dependent ordering transitions. Here, we tackle these challenges by providing a multicomponent thermodynamic modeling framework for FeTi, a representative bcc-derived material class, which is one of the most relevant room-temperature interstitial metal hydrides. We aim specifically to describe para-equilibrium in FeTi-based multicomponent hydrides while ensuring compatibility with previously evaluated metallic systems. DFT point-defect calculations provide a physics-informed foundation to identify substitutional site preferences. Not only does our approach give detailed guidance for the selection of model parameters to evaluate phase equilibria for a broad range of FeTi-based multicomponent systems with high fidelity, but it also can be easily adopted to other interstitial hydrogen storage compounds.

Hydrogen is attracting significant attention as a next-generation energy carrier, particularly due to its high specific energy [1,2]. However, hydrogen gas has a poor volumetric energy density, and compressing or condensing it for storage requires considerable additional work and heat, rendering poor efficiency. As such, solid-state storage in the form of metal hydrides is notably promising [3]. Among metals that reversibly form hydrides, FeTi-based alloys are of particular interest, on account of their reversible hydrogenation at near-ambient temperatures and pressures and readily available constituent elements [4].

Hydrogenation of metals is governed fundamentally by changes in entropy and enthalpy related to the formation of the hydride phase, which determines the temperature and pressure conditions needed during operation [5]. Entropy contributions are primarily due to differences between gas-phase H_2 and atomic hydrogen within the crystal lattice [6]. Meanwhile, the enthalpy of hydrogenation depends mainly on the hydrogen affinity of constituent elements. Compositional tuning through alloying is therefore a valuable tool for tailoring the thermodynamics of these materials for technological use. Multicomponent thermodynamic modeling is a well-suited approach to guide alloy design and to evaluate the role of additives and impurities, including those originating from raw and recycled materials [10,11]. When modeling the thermodynamics of material systems, a primary consideration is how effectively the model can be extrapolated to more complex systems. An example is the two-sublattice bcc order-disorder model [12], which describes both the bcc-derived A2 and B2 phases, containing one and two metal sublattices, respectively [Fig. 1(*a*) and (*b*)], with a single Gibbs energy expression. This model is justified because in many systems (e.g. Al-Fe-Ni [13], Cu-Zn [14], and Fe-Si [15]), the bcc phase can undergo a continuous ordering transition to B2, which characterizes it as a second-order thermodynamic transition. In contrast, the transition in the Fe-Ti system has a first-order character and B2 can be modeled as a unique phase. Nevertheless, the model is usually employed to ensure compatibility and robust extrapolation to higher-order systems [7,16–20].

The hydrogenation of intermetallics often occurs in a state of partial equilibrium known as para-equilibrium. In this state, the alloy's metal composition remains constant due to the sluggish diffusion of metal atoms at hydrogenation temperatures. Thus, only hydrogen equilibrates within the system, meaning that at para-equilibrium, each phase has the

* Corresponding authors.
E-mail addresses: ebert.alvares@hereon.de (E. Alvares), paul.jerabek@hereon.de (P. Jerabek).

https://doi.org/10.1016/j.scriptamat.2024.116516
Received 30 August 2024; Received in revised form 2 December 2024; Accepted 12 December 2024

Available online 16 January 2025

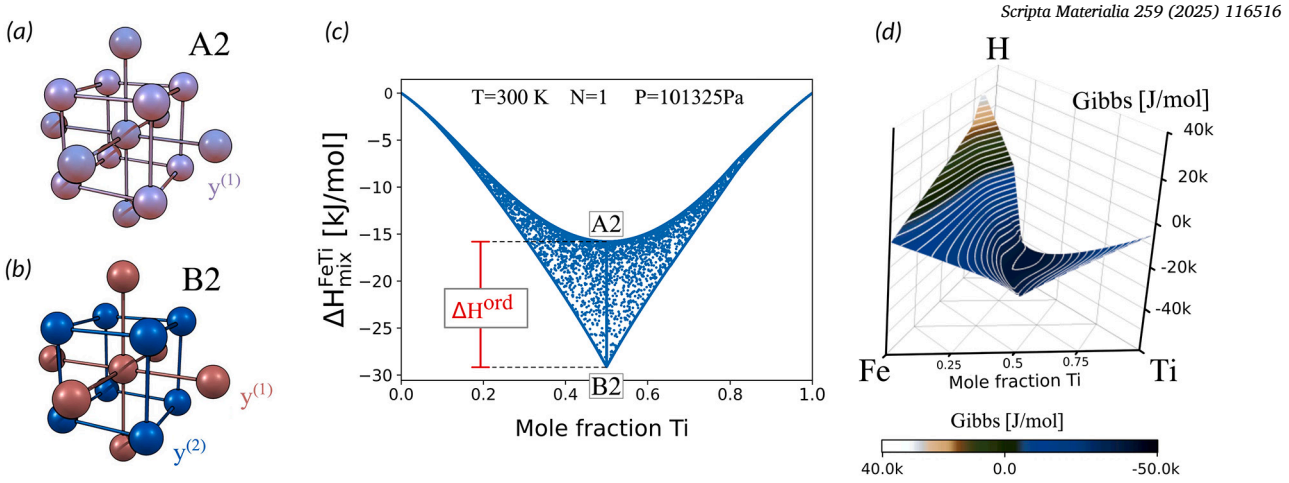

Fig. 1. Structural and thermodynamic properties of the bcc phase of the Fe-Ti-H system using the order-disorder model calculated with parameters from the works of Santhy [7], Ukita [8], and Kim [9]. (*a*) The disordered, A2 bcc phase structure; (*b*) The fully ordered, B2 bcc phase structure; (*c*) Enthalpy of mixing of the bcc phase of the Fe-Ti system at 300 K, highlighting the highest enthalpy of ordering at equimolar composition; (*d*) Gibbs energy surface at 1000 K.

same hydrogen chemical potential, while the chemical potential gradient of metallic species persists.

In AB metal-hydrogen systems, metals A and B are generally selected on the basis of their disparate hydrogen affinities [4], such that their associated binary hydrides are stable under a targeted range of conditions. This disparity in hydrogen affinity makes applying the order-disorder model to para-equilibrium in these systems even more complex. Incorporating interstitial hydrogen into the model must account for both the para-equilibrium state that governs hydrogenation of the intermetallic phase as well as the more stable complete-equilibrium state. This means that for the monohydride FeTiH in the Fe–Ti–H system, equilibrium between the intermetallic Laves phase, Fe_2Ti, and the more stable binary hydride, TiH_2, must be considered. Recently, we proposed the first approach to overcome this problem by treating interstitial hydrogen in the FeTi bcc phase after constraining the metallic form with the analytical derivation of the Gibbs energy for the perfectly ordered state of the bcc order-disorder model, requiring the resulting thermodynamic model to be compatible with the Fe–Ti system [21]. Even so, the successful extrapolation of our model to multicomponent alloys remained elusive [22].

To treat the order-disorder transition in bcc-derived phases [23], the Gibbs energy model assumes two distinct contributions: one from the disordered phase (A2), and another from the energy ΔG^{ord} to form an ordered phase (B2). In the fully disordered state, the metallic sublattices are indistinguishable (i.e. they have identical atomic concentrations), whereas, in the ordered state, two metallic lattices are uniquely defined by their distinct compositions. We denote these two sublattices with superscripts "(1)" and "(2)"; for A2, the single metallic sublattice is labeled "(1)". Hydrogen occupies a third, interstitial sublattice, denoted as "(i)", which can be described by the mixing of hydrogen atoms (H) and unoccupied interstices (□).

The compound energy formalism (CEF) [24,25] sublattice model defines the binary metallic disordered A2 phase, containing elements A and B, as $(\mathrm{A,B})^{(1)}(\mathrm{H},\square)^{(i)}_{b}$, with its Gibbs energy expressed as:

$$
\begin{aligned}
G^{\mathrm{A2}} = {} & y_{\mathrm{A}}^{(1)} y_{\square}^{(\mathrm{i})} G^{\mathrm{A2}}_{\mathrm{A}:\square} + y_{\mathrm{B}}^{(1)} y_{\square}^{(\mathrm{i})} G^{\mathrm{A2}}_{\mathrm{B}:\square} \\
& + y_{\mathrm{A}}^{(1)} y_{\mathrm{H}}^{(\mathrm{i})} G^{\mathrm{A2}}_{\mathrm{A}:\mathrm{H}} + y_{\mathrm{B}}^{(1)} y_{\mathrm{H}}^{(\mathrm{i})} G^{\mathrm{A2}}_{\mathrm{B}:\mathrm{H}} \\
& + RT\left(y_{\mathrm{A}}^{(1)} \ln y_{\mathrm{A}}^{(1)} + y_{\mathrm{B}}^{(1)} \ln y_{\mathrm{B}}^{(1)}\right) \\
& + bRT\left(y_{\square}^{(\mathrm{i})} \ln y_{\square}^{(\mathrm{i})} + y_{\mathrm{H}}^{(\mathrm{i})} \ln y_{\mathrm{H}}^{(\mathrm{i})}\right) \\
& + \sum_{i,j,k} y_i^{(1)} y_j^{(1)} y_k^{(\mathrm{i})} L^{\mathrm{A2}}_{i:j:k} \\
& + \sum_{i,j,k,l} y_i^{(1)} y_j^{(1)} y_k^{(\mathrm{i})} y_l^{(\mathrm{i})} L^{\mathrm{A2}}_{i,j:k,l} + G^{\mathrm{mo}}.
\end{aligned}
\tag{1}
$$

While the B2 phase, $(\mathrm{A,B})^{(1)}_{0.5}(\mathrm{A,B})^{(2)}_{0.5}(\mathrm{H},\square)^{(\mathrm{i})}_{b}$, has its Gibbs energy expressed as:

$$
\begin{aligned}
G^{\mathrm{B2}} = {} & y_{\mathrm{A}}^{(1)} y_{\mathrm{A}}^{(2)} y_{\square}^{(\mathrm{i})} G^{\mathrm{B2}}_{\mathrm{A:A}:\square} + y_{\mathrm{B}}^{(1)} y_{\mathrm{B}}^{(2)} y_{\square}^{(\mathrm{i})} G^{\mathrm{B2}}_{\mathrm{B:B}:\square} \\
& + y_{\mathrm{A}}^{(1)} y_{\mathrm{A}}^{(2)} y_{\mathrm{H}}^{(\mathrm{i})} G^{\mathrm{B2}}_{\mathrm{A:A}:\mathrm{H}} + y_{\mathrm{B}}^{(1)} y_{\mathrm{B}}^{(2)} y_{\mathrm{H}}^{(\mathrm{i})} G^{\mathrm{B2}}_{\mathrm{B:B}:\mathrm{H}} \\
& + y_{\mathrm{A}}^{(1)} y_{\mathrm{B}}^{(2)} y_{\square}^{(\mathrm{i})} G^{\mathrm{B2}}_{\mathrm{A:B}:\square} + y_{\mathrm{B}}^{(1)} y_{\mathrm{A}}^{(2)} y_{\square}^{(\mathrm{i})} G^{\mathrm{B2}}_{\mathrm{B:A}:\square} \\
& + y_{\mathrm{A}}^{(1)} y_{\mathrm{B}}^{(2)} y_{\mathrm{H}}^{(\mathrm{i})} G^{\mathrm{B2}}_{\mathrm{A:B}:\mathrm{H}} + y_{\mathrm{B}}^{(1)} y_{\mathrm{A}}^{(2)} y_{\mathrm{H}}^{(\mathrm{i})} G^{\mathrm{B2}}_{\mathrm{B:A}:\mathrm{H}} \\
& + 0.5RT\left(y_{\mathrm{A}}^{(1)} \ln y_{\mathrm{A}}^{(1)} + y_{\mathrm{B}}^{(1)} \ln y_{\mathrm{B}}^{(1)}\right) \\
& + 0.5RT\left(y_{\mathrm{A}}^{(2)} \ln y_{\mathrm{A}}^{(2)} + y_{\mathrm{B}}^{(2)} \ln y_{\mathrm{B}}^{(2)}\right) \\
& + bRT\left(y_{\square}^{(\mathrm{i})} \ln y_{\square}^{(\mathrm{i})} + y_{\mathrm{H}}^{(\mathrm{i})} \ln y_{\mathrm{H}}^{(\mathrm{i})}\right) \\
& + \sum_{i,j,k,l} y_i^{(1)} y_j^{(1)} y_k^{(2)} y_l^{(\mathrm{i})} L^{\mathrm{B2}}_{i,j:k:l} \\
& + \sum_{i,j,k,l} y_k^{(1)} y_i^{(2)} y_j^{(2)} y_l^{(\mathrm{i})} L^{\mathrm{B2}}_{k:i,j:l} \\
& + \sum_{i,j,k,l} y_i^{(1)} y_j^{(2)} y_k^{(\mathrm{i})} y_l^{(\mathrm{i})} L^{\mathrm{B2}}_{i:j:k,l} \\
& + \sum_{i,j,k,l,m} y_i^{(1)} y_j^{(1)} y_k^{(2)} y_l^{(2)} y_m^{(\mathrm{i})} L^{\mathrm{B2}}_{i,j:k,l:m} \\
& + \sum_{i,j,k,l,m} y_i^{(1)} y_j^{(1)} y_m^{(2)} y_k^{(\mathrm{i})} y_l^{(\mathrm{i})} L^{\mathrm{B2}}_{i,j:m:k,l} \\
& + \sum_{i,j,k,l,m} y_m^{(1)} y_i^{(2)} y_j^{(2)} y_k^{(\mathrm{i})} y_l^{(\mathrm{i})} L^{\mathrm{B2}}_{m:i,j:k,l} + G^{\mathrm{mo}}.
\end{aligned}
\tag{2}
$$

Here, the sublattices are separated by colons (:), while different elements within given sublattices are separated by commas (,). y_i refers to the fraction of element i in a sublattice. $L_{i,j:*}$, $L_{*:i,j}$, $L_{*:i,j:*}$, $L_{i,j:*:*}$, $L_{*:*:i,j}$ are binary interaction parameters, often expressed with temperature-dependent Redlich-Kister polynomials [26], and $L_{i,j:k,l}$, $L_{i,j:k,l:*}$, $L_{i,j:*:k,l}$, $L_{*:i,j:k,l}$ represent reciprocal lattice interaction parameters [12], where * represents any possible element in the sublattice. The term G^{mo} refers to the magnetic ordering as described by the Hillert-Jarl-Inden model [27,28].

When the elemental compositions of the two metallic sublattices are indistinguishable ($y_i^{(1)} = y_i^{(2)} \forall i$), the ordered phase model (B2) becomes

disordered. The ordering contribution is represented by the difference in energy between the ordered ($G^{\mathrm{B2}}_{\mathrm{ord}}$) and disordered ($G^{\mathrm{B2}}_{\mathrm{dis}}$) states:

$$\begin{aligned}\Delta G^{\mathrm{ord}} = & G^{\mathrm{B2}}_{\mathrm{ord}}\left(y^{(1)}_i, y^{(2)}_j, y^{(\mathrm{i})}_k\right) \\ & - G^{\mathrm{B2}}_{\mathrm{dis}}\left(y^{(1)}_i = y^{(2)}_i, y^{(\mathrm{i})}_k\right).\end{aligned} \tag{3}$$

The total free energy of the bcc phase is finally expressed as:

$$G^{\mathrm{bcc}} = G^{\mathrm{A2}} + \Delta G^{\mathrm{ord}}. \tag{4}$$

Due to bcc symmetry, the following model parameters are equivalent:

$$G^{\mathrm{B2}}_{\mathrm{A:B}:i} = G^{\mathrm{B2}}_{\mathrm{B:A}:i}; \tag{5}$$

$$L^{\mathrm{B2}}_{\mathrm{A,B}:i:j} = L^{\mathrm{B2}}_{i:\mathrm{A,B}:j}; \tag{6}$$

$$L^{\mathrm{B2}}_{i:j:\mathrm{H},\square} = L^{\mathrm{B2}}_{j:i:\mathrm{H},\square}. \tag{7}$$

As discussed, complications may arise if the metal elements have vastly different hydrogen affinities. For instance, in the AB-H system, the hydride of element A may be highly unstable ($G^{\mathrm{A2}}_{\mathrm{A:H}} \gg 0$ and/or $L^{\mathrm{A2}}_{A:\square,H} \gg 0$), while the hydride of B may be very stable ($G^{\mathrm{A2}}_{\mathrm{B:H}} \ll 0$ and/or $L^{\mathrm{A2}}_{B:\square,H} \ll 0$). As a result, modeling the interstitial solution within an equimolar AB bcc phase requires a complex combination of the binary and reciprocal lattice interaction parameters. Even if these parameters can be evaluated numerically, their physical meaning is unclear.

Figs. 1(*c*) and (*d*) illustrate the effect of binary parameters on the ternary bcc phase in the Fe-Ti-H system. The stability difference between the binary Ti-H and Fe-H systems complicates the description of para-equilibrium. Fig. 1(*c*) shows the significant binary contributions of the ordering enthalpy that affect the shape of the internal-equilibrium Gibbs energy surface [Fig. 1(*d*)]. The ordering enthalpy (ΔH^{ord}) is maximized for the equimolar composition, favoring the ordered state (B2) over the disordered state (A2). Similarly, the enthalpy of the metal-hydrogen solution shifts the Gibbs energy surface of the bcc phase, maximizing it for the Fe-H binary system, and minimizing it for Ti-H.

Perfect metallic ordering in the bcc phase is achieved when the interstitial lattice is unoccupied, while each metal element occupies a different sublattice. Taking the example of an equimolar composition, the elemental fractions in the single sublattice of the A2 model are $y^{(1)}_{\mathrm{A}} = y^{(1)}_{\mathrm{B}} = 0.5$, $y^{(\mathrm{i})}_{\square} = 1$, and $y^{(\mathrm{i})}_{\mathrm{H}} = 0$. If the equimolar bcc compound is paramagnetic under standard application temperatures (as in the case of bcc FeTi [29]), such that $G^{\mathrm{mo}} \approx 0$, the resulting Gibbs energy expression for the A2 bcc phase (Equation (1)) becomes:

$$\begin{aligned}G^{\mathrm{A2}} = & 0.5 G^{\mathrm{A2}}_{\mathrm{A}:\square} + 0.5 G^{\mathrm{A2}}_{\mathrm{B}:\square} \\ & + RT\left(0.5\ln 0.5 + 0.5\ln 0.5\right) \\ & + 0.25 L^{\mathrm{A2}}_{\mathrm{A,B}:\square}.\end{aligned} \tag{8}$$

For the fully ordered B2 state, two possible symmetrically equivalent configurations generate an equimolar composition, i.e.$(\mathrm{A})^{(1)}_{0.5}(\mathrm{B})^{(2)}_{0.5}(\square)^{(\mathrm{i})}_{b}$, and $(\mathrm{B})^{(1)}_{0.5}(\mathrm{A})^{(2)}_{0.5}(\square)^{(\mathrm{i})}_{b}$. Taking the first configuration as an example, the sublattice compositions are $y^{(1)}_{\mathrm{A}} = y^{(2)}_{\mathrm{B}} = 1$, $y^{(1)}_{\mathrm{B}} = y^{(2)}_{\mathrm{A}} = 0$, $y^{(\mathrm{i})}_{\square} = 1$, and $y^{(\mathrm{i})}_{\mathrm{H}} = 0$. Applying Equation (2) to these configurations leads to a dramatically reduced expression:

$$G^{\mathrm{B2}}_{\mathrm{ord}} = G^{\mathrm{B2}}_{\mathrm{A:B}:\square}. \tag{9}$$

Note that with no mixing in the sublattices, the binary ideal entropy of mixing is zero, i.e. $\lim_{y_i \to 0}\left[y_i \ln y_i + (1-y_i)\ln(1-y_i)\right] = 0$.

For the same composition, in the fully disordered state, the B2 model has equimolar composition in both metallic sublattices: $y^{(1)}_{\mathrm{A}} = y^{(2)}_{\mathrm{A}} = 0.5$, $y^{(1)}_{\mathrm{B}} = y^{(2)}_{\mathrm{B}} = 0.5$, $y^{(\mathrm{i})}_{\square} = 1$, and $y^{(\mathrm{i})}_{\mathrm{H}} = 0$. As a result, Equation (2) leads to:

$$\begin{aligned}G^{\mathrm{B2}}_{\mathrm{dis}} = & + 0.5 G^{\mathrm{B2}}_{\mathrm{A:B}:\square} \\ & + RT\left(0.5\ln 0.5 + 0.5\ln 0.5\right) \\ & + 0.25 L^{\mathrm{B2}}_{\mathrm{A,B:A}:\square} \\ & + 0.25 L^{\mathrm{B2}}_{\mathrm{A,B:B}:\square}.\end{aligned} \tag{10}$$

For equimolar quantities, the Redlich-Kister polynomials [26],

$$L^{\phi}_{i,j} = y_i y_j \sum_{\upsilon=0}^{n} {}^{\upsilon}L^{\phi}_{i,j}\left(y_i - y_j\right)^{\upsilon}, \tag{11}$$

are represented solely by their 0th-order terms, ${}^{0}L^{\phi}_{i,j}$. Additionally, because the ordering contribution is referenced to the disordered phase, by definition, we have $G^{\mathrm{B2}}_{\mathrm{A:A}:\square} = G^{\mathrm{B2}}_{\mathrm{B:B}:\square} = 0$. The phase is instead referenced to the standard element reference (SER) energies through the A2 unary terms ($G^{\mathrm{A2}}_{\mathrm{A}:\square} = G^{\mathrm{bcc}}_{\mathrm{A}} - H^{\mathrm{SER}}_{\mathrm{A}}$, and $G^{\mathrm{A2}}_{\mathrm{B}:\square} = G^{\mathrm{bcc}}_{\mathrm{B}} - H^{\mathrm{SER}}_{\mathrm{B}}$) [30]. Substituting Equations (8), (9), and (10) into Equation (4) then yields the general model for a perfectly ordered AB bcc system from the order-disorder model:

$$\begin{aligned}G^{\mathrm{bcc}}_{\mathrm{A:B}:\square} = & + 0.5^{\circ} G^{\mathrm{bcc}}_{\mathrm{A}} + 0.5^{\circ} G^{\mathrm{bcc}}_{\mathrm{B}} + 0.5 G^{\mathrm{B2}}_{\mathrm{A:B}:\square} \\ & + 0.25\,{}^{0}L^{\mathrm{A2}}_{\mathrm{A,B}:\square} \\ & - 0.25\left({}^{0}L^{\mathrm{B2}}_{\mathrm{A,B:A}:\square} + {}^{0}L^{\mathrm{B2}}_{\mathrm{A,B:B}:\square}\right).\end{aligned} \tag{12}$$

Note that immiscible bcc solutions have not yet been widely assessed in the literature, and appropriate parameters for the order-disorder model are not yet available. Moreover, calculations of hypothetical disordered bcc structures from first-principles are computationally demanding, considering the number of possible microstates for any given phase composition. In this case, however, the ${}^{0}L^{\mathrm{A2}}_{\mathrm{A,B}:\square}$ interaction parameter from Equation (12) can be, as an initial approximation, taken from the Miedema's molar enthalpy of mixing ($\Delta \bar{H}^{\mathrm{Miedema}}_{\mathrm{mix}}$) [31–33]:

$${}^{0}L^{\mathrm{A2}}_{\mathrm{A,B}:\square} = 4\Delta \bar{H}^{\mathrm{Miedema}}_{\mathrm{A,B\ mix}}. \tag{13}$$

We now consider a dilute solution of some substitutional metal element M within an ordered bcc structure containing interstitial hydrogen, which we call α. Equation (12) can be utilized for the end-members of the α phase, helping to describe the impact of adding M on the relevant metallic sites. If M preferentially occupies the same sublattice as A, giving rise to the chemical formula $(\mathrm{A,M})^{(1)}_{0.5}(\mathrm{B})^{(2)}_{0.5}(\mathrm{H},\square)^{(\mathrm{i})}_{b}$, the Gibbs energy can be expressed as:

$$\begin{aligned}G^{\alpha} = & y^{(1)}_{\mathrm{A}} y^{(2)}_{\mathrm{B}} y^{(\mathrm{i})}_{\square} G^{\mathrm{bcc}}_{\mathrm{A:B}:\square} + y^{(1)}_{\mathrm{M}} y^{(2)}_{\mathrm{B}} y^{(\mathrm{i})}_{\square} G^{\mathrm{bcc}}_{\mathrm{M:B}:\square} \\ & + y^{(1)}_{\mathrm{A}} y^{(2)}_{\mathrm{B}} y^{(\mathrm{i})}_{\mathrm{H}} G^{\mathrm{bcc}}_{\mathrm{A:B:H}} + y^{(1)}_{\mathrm{M}} y^{(2)}_{\mathrm{B}} y^{(\mathrm{i})}_{\mathrm{H}} G^{\mathrm{bcc}}_{\mathrm{M:B:H}} \\ & + 0.5 RT\left(y^{(1)}_{\mathrm{A}} \ln y^{(1)}_{\mathrm{A}} + y^{(1)}_{\mathrm{M}} \ln y^{(1)}_{\mathrm{M}}\right) \\ & + bRT\left(y^{(\mathrm{i})}_{\mathrm{H}} \ln y^{(\mathrm{i})}_{\mathrm{H}} + y^{(\mathrm{i})}_{\square} \ln y^{(\mathrm{i})}_{\square}\right) \\ & + y^{(1)}_{\mathrm{A}} y^{(1)}_{\mathrm{M}} y^{(2)}_{\mathrm{B}} y^{(\mathrm{i})}_{\square} L^{\alpha}_{\mathrm{A,M:B}:\square} \\ & + y^{(1)}_{\mathrm{A}} y^{(1)}_{\mathrm{M}} y^{(2)}_{\mathrm{B}} y^{(\mathrm{i})}_{\mathrm{H}} L^{\alpha}_{\mathrm{A,M:B:H}} \\ & + y^{(1)}_{\mathrm{A}} y^{(2)}_{\mathrm{B}} y^{(\mathrm{i})}_{\mathrm{H}} y^{(\mathrm{i})}_{\square} L^{\alpha}_{\mathrm{A:B:H},\square} \\ & + y^{(1)}_{\mathrm{M}} y^{(2)}_{\mathrm{B}} y^{(\mathrm{i})}_{\mathrm{H}} y^{(\mathrm{i})}_{\square} L^{\alpha}_{\mathrm{M:B:H},\square} \\ & + y^{(1)}_{\mathrm{A}} y^{(1)}_{\mathrm{M}} y^{(2)}_{\mathrm{B}} y^{(\mathrm{i})}_{\mathrm{H}} y^{(\mathrm{i})}_{\square} L^{\alpha}_{\mathrm{A,M:B:H},\square}.\end{aligned} \tag{14}$$

Treating the configurational entropy as an ideal mixing of the metals in the first sublattice, i.e. ${}^{\mathrm{cnf}}S_{\mathrm{A,M}} = {}^{\mathrm{id}}S_{\mathrm{A,M}} = R\left(y^{(1)}_{\mathrm{A}} \ln y^{(1)}_{\mathrm{A}} + y^{(1)}_{\mathrm{M}} \ln y^{(1)}_{\mathrm{M}}\right)$, is generally sufficient to describe dilute solutions accurately. In this case, the binary excess contributions $L^{\alpha}_{\mathrm{A,M:B}:i}$ may be neglected, but whether this assumption is reasonable depends on the specific system. The contribution of the interaction expressed by the reciprocal lattice parameter $L_{\mathrm{A,M:B:H},\square}$ is likewise relatively unimportant: because it is multiplied by four fractional values in Equation (14), only an unrealistically large

value would effectively influence the Gibbs energy. Such large values should be avoided during model assessments.

Additionally, the mixing of hydrogen usually deviates from the ideal model due to the site-blocking effect of hydrogen-hydrogen interactions. Recent work demonstrated that the site-blocking effect of unary interstitial element mixing can be more accurately described by the Johnson-Mehl-Avrami-Kolmogorov (JMAK) model [34], which is solely based on the number of sites blocked by the interstitial element. In this case, the terms corresponding to hydrogen's ideal entropy of mixing, $R\left(y_{\mathrm{H}}^{(\mathrm{i})}\ln y_{\mathrm{H}}^{(\mathrm{i})}+y_{\square}^{(\mathrm{i})}\ln y_{\square}^{(\mathrm{i})}\right)$, and excess contributions, $L_{\mathrm{A:B:H,}\square}$ and $L_{\mathrm{M:B:H,}\square}$, should be replaced by the JMAK description.

Lastly, the terms $G_{i:j:\mathrm{H}}^{\mathrm{bcc}}$ represent bcc structured compounds with the interstitial lattice fully occupied by hydrogen and can be expressed with the elemental reference energies as:

$$G_{i:j:\mathrm{H}}^{\mathrm{bcc}}=+0.5\left({}^{\circ}G_{i}^{\mathrm{SER}}+{}^{\circ}G_{j}^{\mathrm{SER}}+b^{\circ}G_{\mathrm{H_2}}^{\mathrm{SER}}\right)+\Delta H_{i:j:\mathrm{H}}^{f}+T\Delta S_{i:j:\mathrm{H}}^{f}. \tag{15}$$

These compounds are generally not stable, making experimental determination of their energetics unfeasible. Instead, their formation enthalpies $\Delta H_{i:j:\mathrm{H}}^{f}$ should be calculated from first principles [35], which results in an error of $\approx$10 kJ mol^{-1} at room temperature [36]. The formation entropy $\Delta S_{i:j:\mathrm{H}}^{f}$, which captures differences between gas-phase H_2 and interstitial hydrogen, can be estimated as 130 J K^{-1} mol^{-1} H_2 [6]. However, this estimate may require further refinement to include secondary entropic contributions [5].

In FeTi, some elements preferentially substitute for either Fe or Ti, while other elements do not have a pronounced site preference. However, allowing the substitutional element M to occupy both sites in the thermodynamic model would require the evaluation of the binary M-H system, due to the additional end-members that must be introduced in Equation (14), i.e. $G_{\mathrm{M:M:}\square}^{\mathrm{bcc}}$, and $G_{\mathrm{M:M:H}}^{\mathrm{bcc}}$. As discussed previously, M metals may have a strong affinity to hydrogen and form highly stable hydrides, leading to $G_{\mathrm{M:H}}^{\mathrm{A2}}\ll 0$ and/or $L_{\mathrm{M:}\square\mathrm{,H}}^{\mathrm{A2}}\ll 0$ and thus reintroducing the problem of describing complete equilibrium and para-equilibrium simultaneously. Therefore, for relevant alloying species, we determine whether there is a preferred sublattice for substitution—and which one if so—by calculating point defect energies from first principles using density functional theory (DFT) [37,38]. Using first-principles calculations to this end provides an invaluable, physics-based foundation for our thermodynamic models, as it is often challenging to discern substitutional preferences from experimental analysis precisely. We employ the generalized gradient approximation of Perdew, Burke, and Ernzerhof (PBE-GGA) to approximate the exchange-correlation functional [39]. More details on the DFT methodology are provided in the Supporting Information (SI).

The formation energy E^f of an elemental defect D in a metallic system is given by [40]:

$$E^f(D)=E(D)-E_{\mathrm{bulk}}+\sum n_{\mathrm{A}}\mu_{\mathrm{A}}. \tag{16}$$

Here, $E(D)$ is the total energy of a supercell containing D, E_{bulk} is the total energy of a pristine supercell, and n_{A} is the number of atoms of element A added ($n_{\mathrm{A}}<0$) or removed ($n_{\mathrm{A}}>0$) to create D. μ_{A} is the chemical potential of A, defined as $\mu_{\mathrm{A}}=E_{\mathrm{tot}}(\mathrm{A})+\Delta\mu_{\mathrm{A}}$, where $E_{\mathrm{tot}}(\mathrm{A})$ is the energy per atom of A in its reference phase, and $\Delta\mu_{\mathrm{A}}$ represents an energy deviation from that reference. To prevent precipitation of the elemental phase, we require that $\Delta\mu_{\mathrm{A}}\leq 0$.

Additional bounds on $\Delta\mu_{\mathrm{A}}$ are set by ensuring thermodynamic stability of the reference phase. For FeTi, this condition corresponds to the equality:

$$\Delta\mu_{\mathrm{Fe}}+\Delta\mu_{\mathrm{Ti}}=\Delta H^{f}(\mathrm{FeTi}), \tag{17}$$

where $\Delta H^{f}(\mathrm{FeTi})$ is the enthalpy of formation of FeTi. We calculate $\Delta H^{f}(\mathrm{FeTi})=-0.83$ eV per formula unit (−40 kJ mol^{-1}), which is slightly larger in magnitude than experimentally reported enthalpies [41] but agrees well with previous computational predictions [42]. Equation (17) allows us to select different chemical potential conditions for calculating formation energies; here, we focus on the Ti-rich ($\Delta\mu_{\mathrm{Ti}}=0$) and Fe-rich ($\Delta\mu_{\mathrm{Fe}}=0$) limits. For each species under consideration, we have calculated the difference in formation energy between substitution on the Ti and Fe sites. These results show quantitatively how much more preferable substitution will be on one sublattice compared to the other, and whether that substitution depends on chemical potential conditions.

Table 1
Relative formation energies of alloying elements D substituting on the Ti and Fe sites in FeTi. ΔE^f is defined as the energy difference $E^f(D_{\mathrm{Ti}})-E^f(D_{\mathrm{Fe}})$, such that a positive value indicates preferential substitution on a Fe site, while a negative value indicates preferential substitution for Ti. The corresponding substitutional site is stated explicitly; in cases where substitution on either site is possible, the more preferred site across the widest range of conditions is indicated in parentheses.

Element	ΔE^f (eV) Ti-rich	ΔE^f (eV) Fe-rich	Site
Al	−0.05	−1.70	Either (Ti)
Ca	−0.50	−2.16	Ti
Co	2.88	1.22	Fe
Cr	1.51	−0.15	Either (Fe)
Cu	1.29	−0.37	Either (Fe)
Li	1.17	−0.48	Either (Fe)
Mg	0.11	−1.55	Either (Ti)
Mn	1.99	0.33	Fe
Ni	2.13	0.48	Fe
Sc	−1.18	−2.83	Ti
Si	0.15	−1.51	Either (Ti)
V	0.09	−1.56	Either (Ti)
Y	−1.49	−3.15	Ti
Zn	0.79	−0.87	Either (Ti)
Zr	−1.61	−3.23	Ti

We visualize our results in Fig. 2 by highlighting elements on the Periodic Table based on their substitutional preference. Elements shaded dark blue or red have a pronounced energetic preference for the Ti or Fe sites, respectively, under all conditions. Lighter-shaded elements still generally prefer one site over the other, but they may substitute on the opposite site under certain conditions, which are difficult to specify precisely because the metal atom chemical potentials defining the "Ti-rich" and "Fe-rich" limits cannot easily be measured in experiments. The formation energy differences underlying our results shown in Fig. 2 are listed in Table 1.

The site preference for incorporation is strongly dependent on the element. Generally, larger species such as Sc, Y, and Zr will prefer to substitute for Ti, while smaller cations such as Mn, Co, and Ni prefer to substitute for Fe. Very similar trends can be found for substitution in the FeTiH monohydride (Table S1) and Fe_2Ti C14 Laves phases (Table S2).

We find that our predicted site preferences align well with previous findings [4,51–53], along with calculated phase diagrams of selected Fe–Ti–M ternary systems (Fig. 3) that are based on compiled experimental and computational data [16–20]. Co, Cr, Mn, and Ni [Fig. 3(*a*)–(*d*)] each display high solubility on the Fe site, based on the continuous, single-phase region for FeTi apparent for a fixed Ti mole fraction of 0.5 (shaded blue). For Co and Ni, this region persists up to complete substitution for Fe. Correspondingly, our calculated relative formation energies in Table 1 show Fe substitution to be preferred for each of these elements; furthermore, we find Co and Ni to have the greatest energetic preference for Fe-site substitution among the elements we consider. Conversely, the phase diagram for Ti–Fe–V [Fig. 3(*e*)] shows solubility of V on both Ti and Fe sites, again agreeing with our formation energy calculations. As an aside, the phase diagrams also show significant solubility on Fe sites in Fe_2Ti Laves phase (magenta shaded regions in Fig. 3), also in agreement with our formation energy calculations (Table S2).

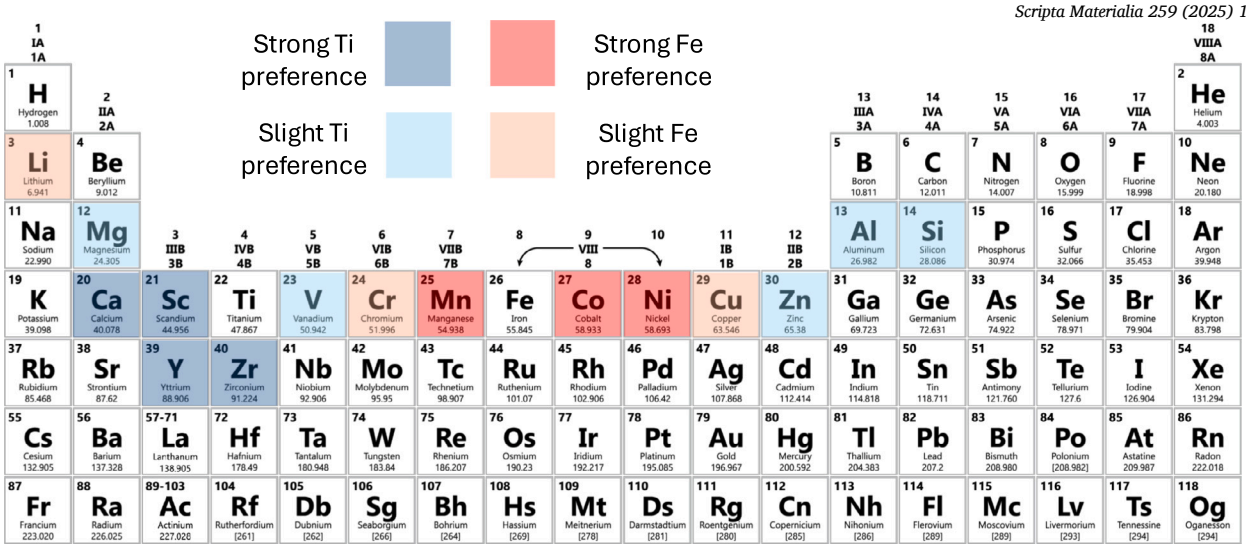

Fig. 2. Periodic Table of the Elements indicating the site preference for substitutional species in FeTi, based on data in Table 1. Blue-shaded elements prefer to substitute for Ti, while red-shaded elements prefer to substitute for Fe. Lighter shading indicates that substitution on the other site may be preferred under certain conditions. For ease of viewing, the lanthanides and actinides are not depicted. (For interpretation of the colors in the figure(s), the reader is referred to the web version of this article.)

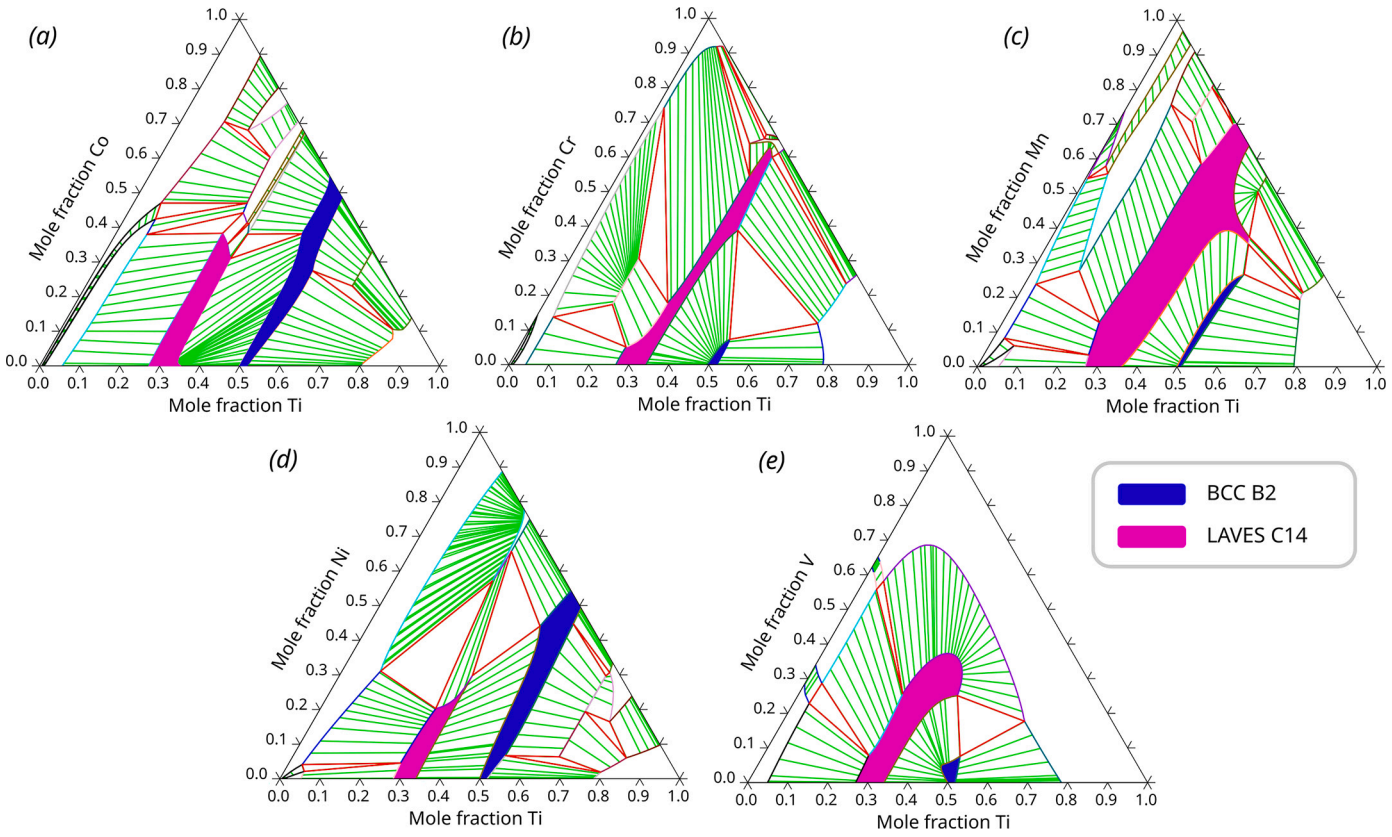

Fig. 3. Calculated Fe–Ti–M ternary phase diagrams at 1273 K using models from: (*a*) M = Co [16]; (*b*) M = Cr [19]; (*c*) M = Mn [18]; (*d*) M = Ni [17]; (*e*) M = V [20]. Continuous, single-phase regions are highlighted for the B2 phase (blue) and C14 Laves phase (magenta).

In accordance with our predicted site preferences, we have collected the parameters necessary to evaluate Equation (12) from thermodynamic data available in the literature. We report these parameters in Table 2 and Table 3 for substitution on the Ti and Fe sublattices, respectively. For V, we provide values both for substitution on the Ti sublattice and on the Fe sublattice, allowing the reader to choose the more relevant site based on the conditions of interest.

We note that these evaluations capture only one end of para-equilibrium, namely, the metallic reference of the ordered bcc alloy. To complete the model for hydrogenation of the AB alloy, a similar procedure must be followed for the hydride phase, ABH. To that end, the formation energies reported in Table S1 can be used to simplify the selection of end-member compounds, and first-principles calculations can be used to compute formation enthalpies (analogously to Equa-

Table 2
Thermodynamic model parameters for Ti-substituting ordered end-members. For conciseness, binary parameters from Equation (12) that were not used in the reference publication are omitted.

Parameter	Value	Ref.
$G^{\mathrm{bcc}}_{\mathrm{Fe:Al:}\square}$	${}^{0}L^{\mathrm{A2}}_{\mathrm{Fe,Al:}\square} = -122960 + 32T$ $G^{\mathrm{B2}}_{\mathrm{Fe:Al:}\square} = -14300$	[43]
$G^{\mathrm{bcc}}_{\mathrm{Fe:Ca:}\square}$	${}^{0}L^{\mathrm{A2}}_{\mathrm{Fe,Ca:}\square} = 110663.41$	[44]
$G^{\mathrm{bcc}}_{\mathrm{Fe:Cu:}\square}$	${}^{0}L^{\mathrm{A2}}_{\mathrm{Fe,Cu:}\square} = -3970.6$	[45]
$G^{\mathrm{bcc}}_{\mathrm{Fe:Mg:}\square}$	${}^{0}L^{\mathrm{A2}}_{\mathrm{Fe,Mg:}\square} = 65700$	[31]
$G^{\mathrm{bcc}}_{\mathrm{Fe:Sc:}\square}$	${}^{0}L^{\mathrm{A2}}_{\mathrm{Fe,Sc:}\square} = -27500$	[46]
$G^{\mathrm{bcc}}_{\mathrm{Fe:Si:}\square}$	${}^{0}L^{\mathrm{A2}}_{\mathrm{Fe,Si:}\square} = -153138.56 + 46.48T$ $G^{\mathrm{B2}}_{\mathrm{Fe:Si:}\square} = -20951.28$	[15]
$G^{\mathrm{bcc}}_{\mathrm{Fe:V:}\square}$	${}^{0}L^{\mathrm{A2}}_{\mathrm{Fe,V:}\square} = -21427 + 6.846T$ $G^{\mathrm{B2}}_{\mathrm{Fe:V:}\square} = 5000$	[20]
$G^{\mathrm{bcc}}_{\mathrm{Fe:Y:}\square}$	${}^{0}L^{\mathrm{A2}}_{\mathrm{Fe,Y:}\square} = 54000$	[47]
$G^{\mathrm{bcc}}_{\mathrm{Fe:Zn:}\square}$	${}^{0}L^{\mathrm{A2}}_{\mathrm{Fe,Zn:}\square} = -1684.72 + 9.92T$	[48]
$G^{\mathrm{bcc}}_{\mathrm{Fe:Zr:}\square}$	${}^{0}L^{\mathrm{A2}}_{\mathrm{Fe,Zr:}\square} = -29828.6 + 6.7520T$	[49]

Table 3
Thermodynamic model parameters for Fe-substituting ordered end-members. For conciseness, binary parameters from Equation (12) that were not used in the reference publication are omitted.

Parameter	Value	Ref.
$G^{\mathrm{bcc}}_{\mathrm{Co:Ti:}\square}$	${}^{0}L^{\mathrm{A2}}_{\mathrm{Co,Ti:}\square} = -92966 + 12.38T$ ${}^{0}L^{\mathrm{B2}}_{\mathrm{Co,Ti:Co:}\square} = -33118$ ${}^{0}L^{\mathrm{B2}}_{\mathrm{Co,Ti:Ti:}\square} = 40388$ $G^{\mathrm{B2}}_{\mathrm{Co:Ti:}\square} = -53950 + 14.03T$	[50]
$G^{\mathrm{bcc}}_{\mathrm{Cr:Ti:}\square}$	${}^{0}L^{\mathrm{A2}}_{\mathrm{Cr,Ti:}\square} = -2247.87 + 9.14T$ $G^{\mathrm{B2}}_{\mathrm{Cr:Ti:}\square} = 82186.5 - 50.5T$	[19]
$G^{\mathrm{bcc}}_{\mathrm{Li:Ti:}\square}$	${}^{0}L^{\mathrm{A2}}_{\mathrm{Li,Ti:}\square} = 136000$	[31]
$G^{\mathrm{bcc}}_{\mathrm{Mn:Ti:}\square}$	${}^{0}L^{\mathrm{A2}}_{\mathrm{Mn,Ti:}\square} = -57924.96$ $G^{\mathrm{B2}}_{\mathrm{Mn:Ti:}\square} = 1321.61$	[18]
$G^{\mathrm{bcc}}_{\mathrm{Ni:Ti:}\square}$	${}^{0}L^{\mathrm{A2}}_{\mathrm{Ni,Ti:}\square} = -97427 + 12.11T$ ${}^{0}L^{\mathrm{B2}}_{\mathrm{Ni,Ti:Ni:}\square} = -55289 + 25.44T$ ${}^{0}L^{\mathrm{B2}}_{\mathrm{Ni,Ti:Ti:}\square} = 60723.7 - 15.40T$ $G^{\mathrm{B2}}_{\mathrm{Ni:Ti:}\square} = -33193.7 + 10.3T$	[17]
$G^{\mathrm{bcc}}_{\mathrm{V:Ti:}\square}$	${}^{0}L^{\mathrm{A2}}_{\mathrm{V,Ti:}\square} = 14000$ $G^{\mathrm{B2}}_{\mathrm{V:Ti:}\square} = 5000$	[20]

tion (15)). Then, after merging these formation enthalpies into the base model for the hydride phase (Equation 6 in Ref. [21])—including previously calculated Gibbs energies and binary interaction parameters as a starting point—the temperature and pressure conditions necessary for para-equilibrium between the metal and its hydride can be estimated. Ultimately, this approach can enable proper evaluation of the role different alloying elements play in determining hydrogen storage properties.

In conclusion, we have proposed a model informed by first-principles calculations that enables the description of para-equilibrium in multicomponent AB metal hydride systems. Our point defect formation energy calculations demonstrated the site preference for different substitutional elements, which in turn determines the appropriate sublattice model for constructing a streamlined thermodynamic reference expression and modeling the Gibbs energy of the ordered bcc phase. We validated the accuracy of these computational predictions through comparison with phase diagrams. Our approach improves the assessment of para-equilibrium conditions by circumventing spurious contributions from the most stable binary bcc hydrides (e.g., Ti–H within the Fe–Ti–H system). The consistency of our proposed models with previously assessed thermodynamic parameters enables the prediction of materials interactions beyond simple chemical intuition. A further advantage of our approach is that it establishes a direct relationship between phase composition and sublattice composition. Such a relationship facilitates the integration of these models into future work in the area of multiscale simulations of metal hydride materials [54–57]. We expect that our model will be valuable for thermodynamic assessments of FeTi-based alloys for hydrogen storage, thereby accelerating their development in large-scale energy storage applications.

CRediT authorship contribution statement

Ebert Alvares: Writing – review & editing, Writing – original draft, Visualization, Software, Methodology, Investigation, Formal analysis, Data curation, Conceptualization. **Andrew J.E. Rowberg:** Writing – review & editing, Writing – original draft, Visualization, Software, Methodology, Investigation, Formal analysis, Data curation. **Kai Sellschopp:** Writing – review & editing, Validation. **Brandon C. Wood:** Writing – review & editing, Supervision, Funding acquisition. **Thomas Klassen:** Writing – review & editing, Supervision, Project administration, Funding acquisition. **Paul Jerabek:** Writing – review & editing, Supervision, Project administration, Funding acquisition. **Claudio Pistidda:** Writing – review & editing, Supervision, Project administration, Funding acquisition.

Declaration of competing interest

The authors declare that they have no known competing financial interests or personal relationships that could have appeared to influence the work reported in this paper.

Acknowledgements

This publication was made possible by the NZMat4H2Sto project, funded by the German Federal Ministry of Education and Research (BMBF). The authors acknowledge support from the Hydrogen Materials Advanced Research Consortium (HyMARC), established as part of the Energy Materials Network by the U.S. Department of Energy (DOE) under Contract DE-AC52-07NA27344, Office of Energy Efficiency and Renewable Energy (EERE), Hydrogen and Fuel Cell Technologies Office. AJER acknowledges the Helmholtz Information & Data Science Academy (HIDA) for providing financial support within the HIDA Trainee Network program to enable a short-term stay at the Helmholtz-Zentrum Hereon. Part of this work was performed under the auspices of the DOE by Lawrence Livermore National Laboratory under Contract DE-AC52-07NA27344. We acknowledge computational resources from the Grand Challenge Program at LLNL. KS was funded by the Deutsche Forschungsgemeinschaft (DFG, German Research Foundation) – 506703280.

Appendix. Supplementary material

Supplementary material related to this article can be found online at https://doi.org/10.1016/j.scriptamat.2024.116516.

References

[1] L. Schlapbach, A. Züttel, Hydrogen-storage materials for mobile applications, Nature 414 (6861) (2001) 353–358, https://doi.org/10.1038/35104634.
[2] C. Pistidda, Solid-state hydrogen storage for a decarbonized society, Hydrogen 2 (4) (2021) 428–443, https://doi.org/10.3390/hydrogen2040024.
[3] J. Bellosta von Colbe, J.-R. Ares, J. Barale, M. Baricco, C. Buckley, G. Capurso, N. Gallandat, D.M. Grant, M.N. Guzik, I. Jacob, E.H. Jensen, T. Jensen, J. Jepsen, T. Klassen, M.V. Lototskyy, K. Manickam, A. Montone, J. Puszkiel, S. Sartori, D.A. Sheppard, A. Stuart, G. Walker, C.J. Webb, H. Yang, V. Yartys, A. Züttel, M. Dornheim,

Application of hydrides in hydrogen storage and compression: achievements, outlook and perspectives, Int. J. Hydrog. Energy 44 (15) (2019) 7780–7808, https://doi.org/10.1016/j.ijhydene.2019.01.104.

[4] E.M. Dematteis, N. Berti, F. Cuevas, M. Latroche, M. Baricco, Substitutional effects in TiFe for hydrogen storage: a comprehensive review, Mater. Adv. 2 (8) (2021) 2524–2560, https://doi.org/10.1039/D1MA00101A.

[5] M. Witman, S. Ling, D.M. Grant, G.S. Walker, S. Agarwal, V. Stavila, M.D. Allendorf, Extracting an empirical intermetallic hydride design principle from limited data via interpretable machine learning, J. Phys. Chem. Lett. 11 (1) (2020) 40–47, https://doi.org/10.1021/acs.jpclett.9b02971.

[6] J.-M. Joubert, CALPHAD modeling of metal–hydrogen systems: a review, JOM 64 (2012) 1438–1447, https://doi.org/10.1007/s11837-012-0462-6.

[7] K. Santhy, K. Hari Kumar, Thermodynamic modelling of magnetic laves phase in Fe–Ti system using first principle method, Intermetallics 128 (2021) 106978, https://doi.org/10.1016/j.intermet.2020.106978.

[8] S. Ukita, H. Ohtani, M. Hasebe, Thermodynamic analysis of the Ti-H and Zr-H binary phase diagrams, Nippon Kinzoku Gakkaishi/J. Jpn Inst. Met. 71 (9) (2007) 721–729, https://doi.org/10.2320/jinstmet.71.721.

[9] K.-H. Kim, J.-H. Shim, B.-J. Lee, Effect of alloying elements (Al, Co, Fe, Ni) on the solubility of hydrogen in vanadium: a thermodynamic calculation, in: 7th Petite Workshop on the Defect Chemical Nature of Energy Materials, 14-17 March 2011, Storaas, Kongsberg, Norway, Int. J. Hydrog. Energy 37 (9) (2012) 7836–7847, https://doi.org/10.1016/j.ijhydene.2012.01.117.

[10] L. Pasquini, K. Sakaki, E. Alvares, P. Jerabek, C. Pistidda, B.C. Wood, et al., Magnesium- and intermetallic alloys-based hydrides for energy storage: modelling, synthesis and properties, Prog. Energy 4 (3) (2022) 032007, https://doi.org/10.1088/2516-1083/ac7190.

[11] Y. Shang, S. Liu, Z. Liang, F. Pyczak, Z. Lei, T. Heidenreich, A. Schökel, J.-j. Kai, G. Gizer, M. Dornheim, T. Klassen, C. Pistidda, Developing sustainable FeTi alloys for hydrogen storage by recycling, Commun. Mater. 3 (1) (2022) 101, https://doi.org/10.1038/s43246-022-00324-5.

[12] H.L. Lukas, S.G. Fries, B. Sundman, Computational Thermodynamics: The Calphad Method, Cambridge University Press, 2007.

[13] L. Zhang, Y. Du, Thermodynamic description of the Al–Fe–Ni system over the whole composition and temperature ranges: modeling coupled with key experiment, Calphad 31 (4) (2007) 529–540, https://doi.org/10.1016/j.calphad.2007.03.003.

[14] W. Gierlotka, S.-w. Chen, Thermodynamic descriptions of the Cu–Zn system, J. Mater. Res. 23 (1) (2008) 258–263, https://doi.org/10.1557/JMR.2008.0035.

[15] J. Lacaze, B. Sundman, An assessment of the Fe-C-Si system, Metall. Trans. A 22 (10) (1991) 2211–2223, https://doi.org/10.1007/BF02664987.

[16] Y. Pan, C. Chen, Y. Du, C. Yuan, F. Luo, Experimental investigation and thermodynamic calculations of the Co-Fe-Ti system, J. Phase Equilib. Diffus. 38 (1) (2017) 5–16, https://doi.org/10.1007/s11669-016-0505-8.

[17] J. De Keyzer, G. Cacciamani, N. Dupin, P. Wollants, Thermodynamic modeling and optimization of the Fe–Ni–Ti system, Calphad 33 (1) (2009) 109–123, https://doi.org/10.1016/j.calphad.2008.10.003, Experimental and Computational investigation of intermetallic systems: a Special Issue Dedicated to Prof. Riccardo Ferro.

[18] A. Walnsch, A. Leineweber, M.J. Kriegel, A third generation CalPhaD assessment of the Fe–Mn–Ti system Part II: the ternary system Fe–Mn–Ti, Calphad 81 (2023) 102553, https://doi.org/10.1016/j.calphad.2023.102553.

[19] S. Wang, K. Wang, G. Chen, Z. Li, Z. Qin, X. Lu, C. Li, Thermodynamic modeling of Ti-Fe-Cr ternary system, Calphad 56 (2017) 160–168, https://doi.org/10.1016/j.calphad.2016.12.007.

[20] C. Guo, C. Li, X. Zheng, Z. Du, Thermodynamic modeling of the Fe–Ti–V system, Calphad 38 (2012) 155–160, https://doi.org/10.1016/j.calphad.2012.06.010.

[21] E. Alvares, P. Jerabek, Y. Shang, A. Santhosh, C. Pistidda, T.W. Heo, B. Sundman, M. Dornheim, Modeling the thermodynamics of the FeTi hydrogenation under para-equilibrium: an ab-initio and experimental study, Calphad 77 (2022) 102426, https://doi.org/10.1016/J.CALPHAD.2022.102426.

[22] M. Palumbo, E.M. Dematteis, L. Fenocchio, G. Cacciamani, M. Baricco, Advances in CALPHAD methodology for modeling hydrides: a comprehensive review, J. Phase Equilib. Diffus. (2024), https://doi.org/10.1007/s11669-024-01113-y.

[23] N. Dupin, I. Ansara, On the sublattice formalism applied to the B2 phase, Int. J. Mater. Res. 90 (1) (1999) 76–85, https://doi.org/10.1515/ijmr-1999-900114.

[24] B. Sundman, J. Ågren, A regular solution model for phases with several components and sublattices, suitable for computer applications, J. Phys. Chem. Solids 42 (4) (1981) 297–301, https://doi.org/10.1016/0022-3697(81)90144-X.

[25] M. Hillert, The compound energy formalism, J. Alloys Compd. 320 (2) (2001) 161–176, https://doi.org/10.1016/S0925-8388(00)01481-X, Materials Constitution and Thermochemistry. Examples of Methods, Measurements and Applications. In Memoriam Alan Prince.

[26] O. Redlich, A.T. Kister, Algebraic representation of thermodynamic properties and the classification of solutions, Ind. Eng. Chem. 40 (2) (1948) 345–348, https://doi.org/10.1021/ie50458a036.

[27] M. Hillert, M. Jarl, A model for alloying in ferromagnetic metals, Calphad 2 (3) (1978) 227–238, https://doi.org/10.1016/0364-5916(78)90011-1.

[28] G. Inden, The role of magnetism in the calculation of phase diagrams, Phys. B+C 103 (1) (1981) 82–100, https://doi.org/10.1016/0378-4363(81)91004-4.

[29] T. Saito, Magnetic properties of Ti–Fe alloy powders prepared by mechanical grinding, J. Alloys Compd. 364 (1) (2004) 113–116, https://doi.org/10.1016/S0925-8388(03)00532-2.

[30] A.T. Dinsdale, SGTE data for elements, Calphad 15 (4) (1991) 317–425, https://doi.org/10.1016/0364-5916(91)90030-N.

[31] Y. Shang, Z. Lei, E. Alvares, S. Garroni, T. Chen, R. Dore, M. Rustici, S. Enzo, A. Schökel, Y. Shi, P. Jerabek, Z. Lu, T. Klassen, C. Pistidda, Ultra-lightweight compositionally complex alloys with large ambient-temperature hydrogen storage capacity, Mater. Today 67 (2023) 113–126, https://doi.org/10.1016/j.mattod.2023.06.012.

[32] M. Poletti, L. Battezzati, Electronic and thermodynamic criteria for the occurrence of high entropy alloys in metallic systems, Acta Mater. 75 (2014) 297–306, https://doi.org/10.1016/j.actamat.2014.04.033.

[33] A.R. Miedema, F.R. de Boer, R. Boom, Model predictions for the enthalpy of formation of transition metal alloys, Calphad 1 (4) (1977) 341–359, https://doi.org/10.1016/0364-5916(77)90011-6.

[34] O.A. Pedroso, Y. Champion, W.J. Botta, G. Zepon, Johnson–Mehl–Avrami–Kolmogorov model applied to describe the site blocking effect in interstitial solid solution, Acta Mater. 271 (2024) 119907, https://doi.org/10.1016/j.actamat.2024.119907.

[35] B.P. Burton, N. Dupin, S.G. Fries, G. Grimvall, A.F. Guillermet, P. Miodownik, W.A. Oates, V. Vinograd, Using ab initio calculations in the calphad environment, Int. J. Mater. Res. 92 (6) (2001) 514–525, https://doi.org/10.3139/ijmr-2001-0105.

[36] S.V. Alapati, J. Karl Johnson, D.S. Sholl, Using first principles calculations to identify new destabilized metal hydride reactions for reversible hydrogen storage, Phys. Chem. Chem. Phys. 9 (2007) 1438–1452, https://doi.org/10.1039/B617927D.

[37] P. Hohenberg, W. Kohn, Inhomogeneous electron gas, Phys. Rev. 136 (1964) B864, https://doi.org/10.1103/PhysRev.136.B864.

[38] W. Kohn, L.J. Sham, Self-consistent equations including exchange and correlation effects, Phys. Rev. 140 (4) (1965) A1133–A1138, https://doi.org/10.1103/PhysRev.140.A1133.

[39] J.P. Perdew, K. Burke, M. Ernzerhof, Generalized gradient approximation made simple, Phys. Rev. Lett. 77 (1996) 3865–3868, https://doi.org/10.1103/PhysRevLett.77.3865.

[40] C. Freysoldt, B. Grabowski, T. Hickel, J. Neugebauer, G. Kresse, A. Janotti, C.G. Van de Walle, First-principles calculations for point defects in solids, Rev. Mod. Phys. 86 (1) (2014) 253, https://doi.org/10.1103/RevModPhys.86.253.

[41] J.C. Gachon, M. Notin, J. Hertz, The enthalphy of mixing of the intermediate phases in the systems FeTi, CoTi, and NiTi by direct reaction calorimetry, Thermochim. Acta 48 (1–2) (1981) 155–164, https://doi.org/10.1016/0040-6031(81)87031-1.

[42] A. Jain, S.P. Ong, G. Hautier, W. Chen, W.D. Richards, S. Dacek, S. Cholia, D. Gunter, D. Skinner, G. Ceder, K.A. Persson, Commentary: the materials project: a materials genome approach to accelerating materials innovation, APL Mater. 1 (1) (2013) 011002, https://doi.org/10.1063/1.4812323.

[43] Z.-K. Liu, Y.A. Chang, Thermodynamic assessment of the Al-Fe-Si system, Metall. Mater. Trans. A 30 (4) (1999) 1081–1095, https://doi.org/10.1007/s11661-999-0160-3.

[44] S. Cui, M. Paliwal, I.-H. Jung, Thermodynamic optimization of Ca-Fe-Si system and its applications to metallurgical grade Si-refining process, Metall. Mater. Trans. E 1 (1) (2014) 67–79, https://doi.org/10.1007/s40553-014-0010-0.

[45] H. Yang, B. Zeng, H. Wang, H. Jin, C. Zhou, Phase equilibria and thermodynamic re-assessment of the Cu–Ti system, Calphad 82 (2023) 102594, https://doi.org/10.1016/j.calphad.2023.102594.

[46] X. Liu, P. Yu, C. Wang, K. Ishida, Thermodynamic evaluation of the Co–Sc and Fe–Sc systems, J. Alloys Compd. 466 (1) (2008) 169–175, https://doi.org/10.1016/j.jallcom.2007.11.069.

[47] I. Saenko, O. Fabrichnaya, A. Udovsky, New thermodynamic assessment of the Fe-Y system, J. Phase Equilib. Diffus. 38 (5) (2017) 684–699, https://doi.org/10.1007/s11669-017-0574-3.

[48] W. Xiong, Y. Kong, Y. Du, Z.-K. Liu, M. Selleby, W.-H. Sun, Thermodynamic investigation of the galvanizing systems, I: refinement of the thermodynamic description for the Fe–Zn system, Calphad 33 (2) (2009) 433–440, https://doi.org/10.1016/j.calphad.2009.01.002, tools for Computational Thermodynamics.

[49] C. Guo, Z. Du, C. Li, B. Zhang, M. Tao, Thermodynamic description of the Al–Fe–Zr system, Calphad 32 (4) (2008) 637–649, https://doi.org/10.1016/j.calphad.2008.08.007.

[50] A.V. Davydov, U.R. Kattner, D. Josell, R.M. Waterstrat, W.J. Boettinger, J.E. Blendell, A.J. Shapiro, Determination of the CoTi congruent melting point and thermodynamic reassessment of the Co-Ti system, Metall. Mater. Trans. A 32 (9) (2001) 2175–2186, https://doi.org/10.1007/s11661-001-0193-8.

[51] W.-S. Ko, K.B. Park, H.-K. Park, Density functional theory study on the role of ternary alloying elements in TiFe-based hydrogen storage alloys, J. Mater. Sci. Technol. 92 (2021) 148–158, https://doi.org/10.1016/j.jmst.2021.03.042.

[52] E.M. Dematteis, D.M. Dreistadt, G. Capurso, J. Jepsen, F. Cuevas, M. Latroche, Fundamental hydrogen storage properties of TiFe-alloy with partial substitution of Fe by Ti and Mn, J. Alloys Compd. 874 (2021) 159925, https://doi.org/10.1016/j.jallcom.2021.159925.

[53] E.M. Dematteis, J. Barale, G. Capurso, S. Deledda, M.H. Sørby, F. Cuevas, M. Latroche, M. Baricco, In-situ neutron diffraction during reversible deuterium loading in Ti-rich and Mn-substituted Ti(Fe, Mn)0.90 alloys, J. Alloys Compd. 935 (2023) 168150, https://doi.org/10.1016/j.jallcom.2022.168150.

[54] E. Alvares, K. Sellschopp, B. Wang, S. Kang, T. Klassen, B.C. Wood, T.W. Heo, P. Jerabek, C. Pistidda, Multiscale modeling of metal-hydride interphases—quantification of decoupled chemo-mechanical energies, npj Comput. Mater. 10 (1) (2024) 249, https://doi.org/10.1038/s41524-024-01424-1.

[55] Y.A. Coutinho, A. Kunwar, N. Moelans, Phase-field approach to simulate BCC-B2 phase separation in the AlnCrFe2Ni2 medium-entropy alloy, J. Mater. Sci. 57 (23) (2022) 10600–10612, https://doi.org/10.1007/s10853-022-07058-2.

[56] D. Schwen, C. Jiang, L. Aagesen, A sublattice phase-field model for direct calphad database coupling, Comput. Mater. Sci. 195 (2021) 110466, https://doi.org/10.1016/j.commatsci.2021.110466.

[57] T. Heo, K. Colas, A. Motta, L.-Q. Chen, A phase-field model for hydride formation in polycrystalline metals: application to δ-hydride in zirconium alloys, Acta Mater. 181 (2019) 262–277, https://doi.org/10.1016/j.actamat.2019.09.047.